Ding et al. Nanoscale Research Letters (2017) 12:63
DOI 10.1186/s11671-017-1852-z

Nanoscale Research Letters

NANO EXPRESS Open Access

The Influence of Hafnium Doping on Density of States in Zinc Oxide Thin-Film Transistors Deposited via Atomic Layer Deposition

Xingwei Ding[1,2], Cunping Qin[2], Jiantao Song[1], Jianhua Zhang[1,2*], Xueyin Jiang[3] and Zhilin Zhang[1,3]

Abstract

Thin-film transistors (TFTs) with atomic layer deposition (ALD) HfZnO (HZO) as channel layer and Al_2O_3 as gate insulator were successfully fabricated. Compared with ZnO-TFT, the stability of HZO-TFT was obviously improved as Hf doping can suppress the generation of oxygen related defects. The transfer characteristics of TFTs at different temperatures were also investigated, and temperature stability enhancement was observed for the TFT with Hf doping. The density of states (DOS) was calculated based on the experimentally obtained E_a, which can explain the experimental observation. A high-field effect mobility of 9.4 cm^2/Vs, a suitable turn-on voltage of 0.26 V, a high on/off ratio of over 10^7 and a steep sub-threshold swing of 0.3 V/decade were obtained in HZO-TFT. The results showed that temperature stability enhancement in HfZnO thin-film transistors are attributed to the smaller DOS.

Background

ZnO-based thin-film transistors (TFT) have recently attracted a great deal of attention owing to their potential application in active matrix liquate crystal display (AMLCD) and active matrix organic light emitting diodes (AMOLED) [1–3]. As an important part of TFTs, channel layers play a crucial role in TFT performance. ZnO-based single channel layer or double channel layer, such as HZO [4], IGZO [5], and IZO/IGZO [6], has been investigated for use in TFTs because of their high mobility. Among those ZnO-based TFTs, amorphous indium-gallium-tin oxide (IGZO) TFTs are regarded as the most promising devices as indium and gallium have excellent lattice matching with ZnO and gallium could suppress carrier generation via oxygen vacancy formation in IGZO. Recently, LG Display has released a 55 in, full high-definition (FHD) OLED television which utilizes an IGZO TFT active matrix [7]. However, materials such as indium (In) and gallium (Ga) have some disadvantages, including toxicity, element scarcity, and indium extraction in hydrogen plasma [8]. Specifically, the instability of ZnO-based TFTs is still a problem hard to solve, as ZnO-based TFTs usually contain defects in the active channel layer and deep-level defects in the channel/insulator interface [9]. To obtain highly stable Zn-based oxide TFTs, many studies have been devoted to the development of robust active layers by the incorporation of metal cations (such as Ga, Al, Hf, and Si) based on sputtering method or spin-coating method [10–14], with the expectation to reduce the density of defects such as oxygen vacancies. There are few reports on adopting ALD method to realize doping in Zn-based oxide TFTs. As it is known, ALD offers various advantages including accurate thickness and composition control, excellent uniformity and step coverage, low defect density, low deposition temperatures, and good reproducibility [15–17]. Furthermore, due to the self-limiting and layer-by-layer (or "digital") growth, ALD exhibits the unique in situ atomic layer doping capability of achieving precise doping with atomic level control during the deposition process.

* Correspondence: dxw1026@126.com
[1]Key Laboratory of Advanced Display and System Application, Ministry of Education, Shanghai University, 149 Yanchang Road, Jingan District, Shanghai 200070, People's Republic of China
[2]School of Mechatronics and Automation, Shanghai University, Shanghai 200072, China
Full list of author information is available at the end of the article

Up to now, to our limited knowledge, the deposition of channel layers using ALD has been focused on almost pure ZnO layers. Given its low standard electrode potential, Hf is a more efficient suppressor of the generation of oxygen vacancies. Adding Hf element could suppress the growth of columnar structure, and therefore drastically decrease the carrier concentration and hall mobility in HZO films [18–20]. Hence, in this paper, Hf doped ZnO has been deposited via ALD and applied in TFTs as channel layer. The related parameters such as the Hf contents, growth temperature, channel thickness, and width/length ratio ($W = L$) were evaluated and optimized. The influence of Hf doping on performance of ZnO-TFT was studied. Especially, the detailed effect of Hf doping on the DOS has never been addressed. In the present letter, the DOS was calculated based on the experimentally obtained E_a, which can explain the experimental observation.

Methods

Bottom-gate TFTs were fabricated on a doped n-type Si wafer as shown in Fig. 1a. Before being placed in the ALD chamber, the Si substrates were cleaned with consecutive rinses of acetone, isopropyl alcohol, and de-ionized water in an ultrasonicator for 15 min, and then treated by Ozone for 10 min. Immediately following this procedure, Al_2O_3 films of approximately 100-nm-thick were deposited by ALD (TFS-200) technique at 240 °C using $Al(CH_3)_3$ and H_2O. The carried gas was nitrogen of 300 sccm. The purge/pluse time for TMA or H_2O was 7/0.1 s. High-purity diethylzinc (DEZn), tetrakisethylmethylamino-hafnium (TEMAHf) were used as Zn, Hf source and water (H_2O) as oxygen source at deposition temperatures of 150 °C. The detailed ALD method to deposit ZnO and Hf dop ZnO films was shown in Fig. 1b. The growth rate of ZnO and HfO_2 films were 0.2 and 0.08 nm/cycle, respectively. Al films deposited by thermal evaporation were used for source/drain electrodes through a shadow-mask with the channel width $W = 1000$ μm and channel length $L = 60$ μm. Thermal annealing was performed in ambient air at 250 °C for 20 min. The structural property of the films was measured with X-ray diffraction measurements with Cu-Kα radiation (D/MAX). Optical transmission was measured using a double beam spectrophotometer (U-3900). The electrical properties were performed using semiconductor parameter analyzer (Agilent, 4155C) with a probe station (LakeShore, TTP4).

Results and Discussion

Figure 2 demonstrates the XRD patterns of ZnO-TFT and HZO-TFT on Si water. The predominant diffraction peaks correspond to the (002) orientation, which indicates that this film has a c-axis orientation polycrystalline structure regardless of Hf insertion. A similar result was obtained by Kim et al. [21]

Figure 3 shows the transmittance spectra of Al_2O_3 (100 nm)-ZnO (40 nm) and Al_2O_3 (100 nm)-HZO (40 nm) deposited on glass at an annealing temperatures of 250 °C for 20 min. The thin films show good transparency of over 95% within the visible light wavelength

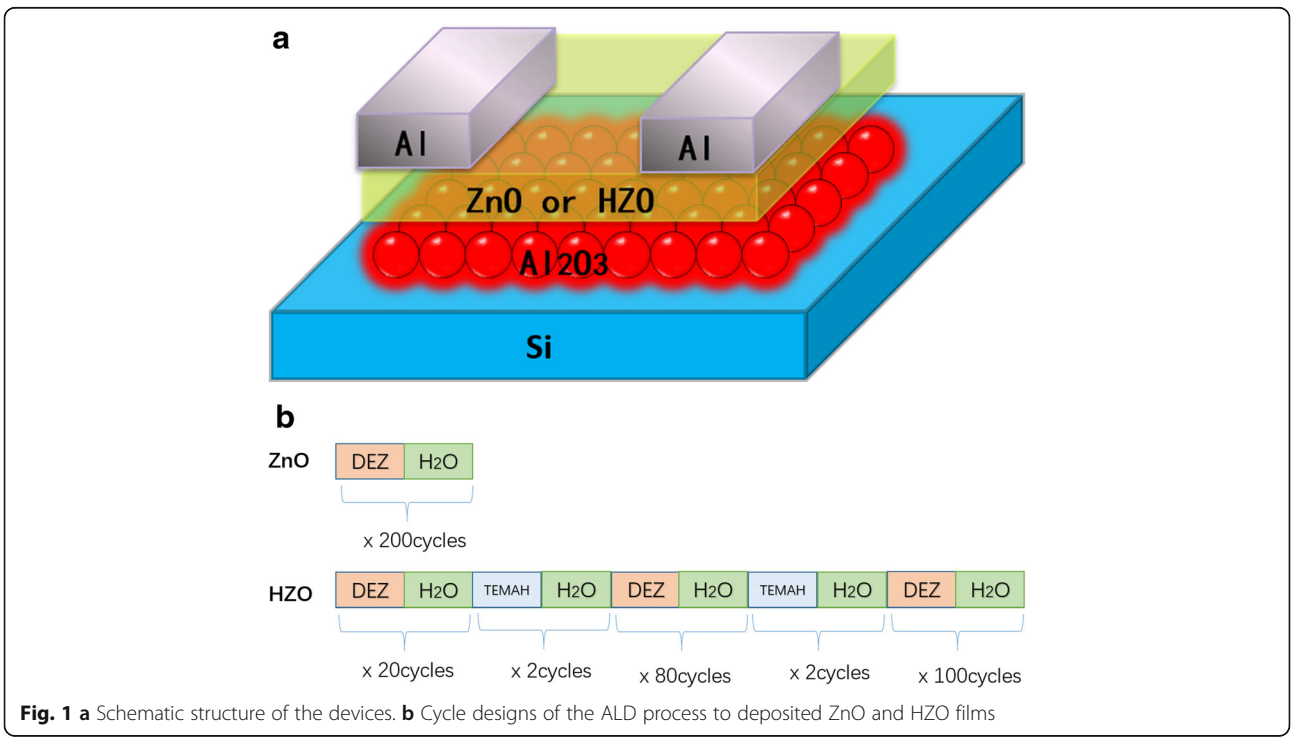

Fig. 1 **a** Schematic structure of the devices. **b** Cycle designs of the ALD process to deposited ZnO and HZO films

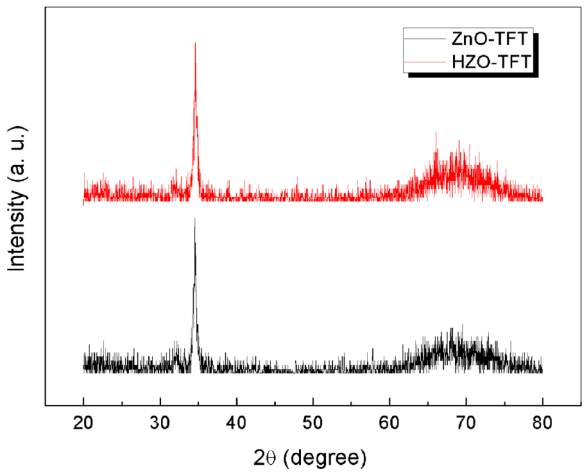

Fig. 2 XRD patterns of ZnO-TFT and HZO-TFT on Si water

range. The absorption edge shows a blue shift with the addition of Hf, consistent with the results for HfZnO prepared by other deposition techniques [22, 23].

Figure 4 shows the transfer curves of ZnO-TFT and HZO-TFT, and their related parameters are summarized in Table 1, including turn-on voltages (Von), field-effect mobility (μ), on/off ratio, and sub-threshold swing (SS). As seen in Table 1, a remarkable improvement in on/off ratio for HZO-TFT was achieved. The on/off-current ratio of the two devices were all over 10^6, indicating that these devices have good characteristics as the backplane of OLEDs requiring a relatively high on-current and small off-current for a rapid response and low power consumption. The SS decreased from 0.4 to 0.3 V/decade. The SS is extracted at the steepest point of the $\log(I_{DS})$-V_{GS} plot by the equation: $SS = dV_{GS}/d(\log I_{DS})$. In addition, the field-effect mobility also decreased from 11.3 to 9.4 cm^2/Vs, and V_{on} increased from 0 to 0.2 V by

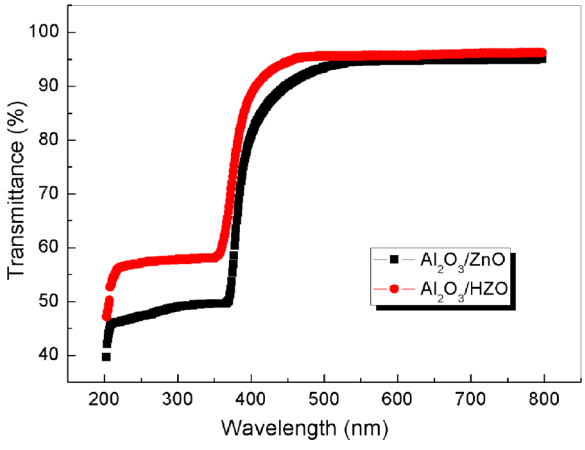

Fig. 3 Transmittance spectra of Al_2O_3 (100 nm)-ZnO (40 nm) and Al_2O_3 (100 nm)-HZO (40 nm) deposited on glass

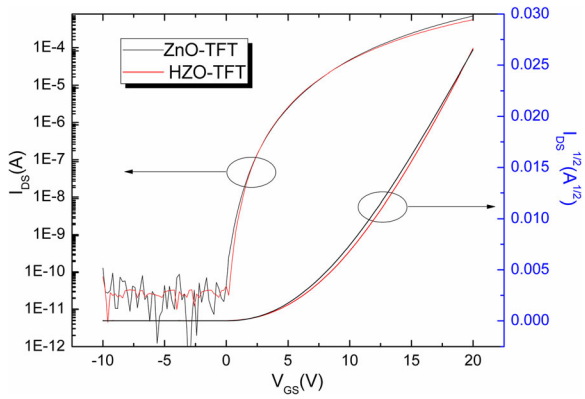

Fig. 4 The transfer curves for the ZnO-TFT and HZO-TFT

the Hf doping. These values for HZO-TFT are comparable to or even exceed the values reported by other HZO-TFTs [12, 21, 24] and much better than those fabricated by ALD [12]. In general, oxide semiconductors containing heavy metal cations with $(n-1)\ d^{10}\ ns^0$ ($n \geq 4$) electronic configurations show high electron mobility as the ns^0 orbitals are overlapped with each other. However, although Hf has a large diameter and the spherical symmetry of the ns^0 orbitals was incorporated, the field-effect mobility and drain current decreased as the Hf content increased. This suggests that Hf ions have a higher oxygen binder energy than that of Zn ions. This can be attributed to the fact that Hf ions have a high electronegativity of 1.3. The field-effect mobility is affected by shallow traps near the conduction band and the interaction of oxygen vacancies, and zinc interstitials is an important source of n-type conductivity in ZnO [25, 26]. Therefore, suppressing the generation of oxygen-vacancy-related defects with Hf doping can effectively decrease the mobility [25]. Decrease in the SS value of HZO-TFT indicates a reduction in interface trap density.

In order to demonstrate the Hf doping on the trap density of states, the temperature-dependent field-effect measurement was used to calculate DOS. Figure 5a, b shows the I_{DS}-V_{GS} curves of ZnO-TFT and HZO-TFT, respectively, as a function of the measurement temperature. The transfer measurement was carried out in the dark after the temperature had been staying at the fixed level for about 1 min. At increasing measurement temperature, all TFTs showed a negative shift of V_{on}. It is well known for the oxide semiconductors materials

Table 1 Comparison of the electrical properties of the devices

Device	V_{on} (V)	μ (cm^2/Vs)	On/off	SS (V/decade)
ZnO-TFT	0	11.3	$>10^6$	0.4
HZO-TFT	0.26	9.4	$>10^7$	0.3

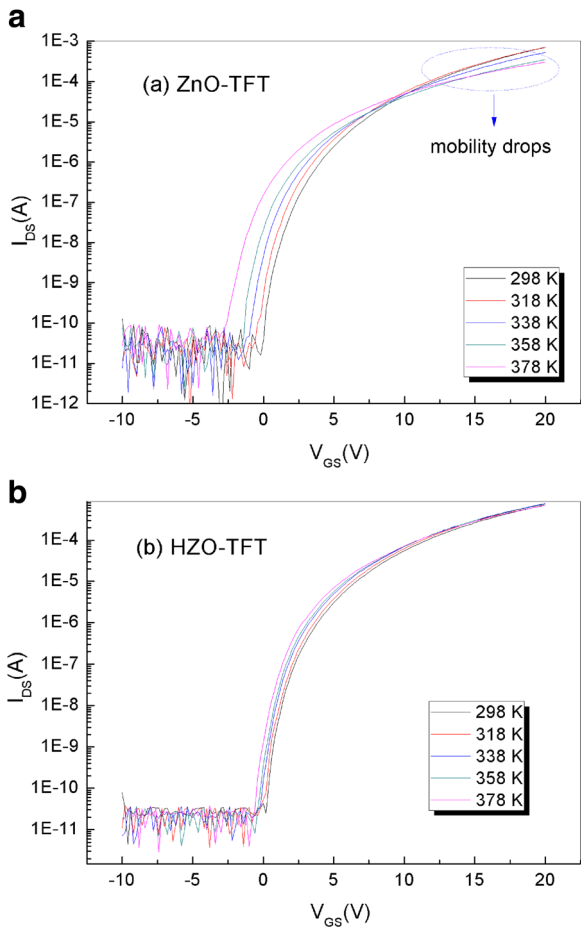

Fig. 5 I_{DS}-V_{GS} curves of **a** ZnO-TFT and **b** HZO-TFT at the different temperatures

that the free electrons mainly result from the detrapping from sub-bandgap trap states and the generation of oxygen vacancies [27–29]. Thermally excited electrons are detrapped from relatively shallow sub-bandgap trap states. In addition, more oxygen vacancies were induced by thermal excitation, and therefore, more free electrons were generated. The lower V_{on} observed at the higher temperature can be attributed to these free electrons from the sub-bandgap trap states which were generated along with the oxygen vacancies [30]. One interesting point to note from our experiment is that the mobility of ZnO-TFT decreased as the temperature increased. The drop in mobility at higher temperature is likely due to the generation of more trap states; as a result, the mobility starts decreasing. Indluru et al. have also observed a similar trend for their a-Si:H TFTs for operation temperatures higher than 348 K [31].

In the sub-threshold region, the current of the TFT devices was well described by the Arrhenius thermal activation model [32, 33]:

$$I_{DS} = I_{D0} \cdot \exp\left[-\frac{E_a(V_{GS})}{kT}\right] \quad (1)$$

where I_{D0} is the prefactor, E_a is the activation energy, k is the Boltzmann constant, and T is the temperature. E_a can be easily extracted by plotting log (I_{DS}) and 1/kT (not shown here).

The relationship between E_a and V_{GS} is shown in Fig. 6. E_a ($E_a = E_C - E_F$) represents the energy difference between the Fermi level (E_F) and the conduction band edge. The falling rates ($d(E_a)/d(V_{GS})$) of ZnO-TFT and HZO-TFT are 0.59 and 0.65 eV/V, respectively. Since the falling rate of E_a with respect to V_{GS} should have the same magnitude as the rate of rising in E_F, the rate-limiting process is the thermal excitation of the trapped charge. All the trap sites below E_F must be filled with electrons before any move to the E_F level in the forbidden bandgap region, so the rate of change in E_F with respect to V_{GS} ($d(E_a)/d(V_{GS})$) is roughly inversely proportional to the magnitude of the total trap density, including the DOS of a semiconductor film (N_{SS}) and an interfacial trap density (N_{it}). Therefore, a much faster falling rate of HZO-TFT compared to ZnO-TFT suggests that a N_{total} value of HZO-TFT is reduced compared to ZnO-TFT. HZO-TFT exhibits a faster moving E_F level with respective V_{GS}, which means the reduction in bulk and interface trap density.

To investigate in detail the distribution and density of tail states and deep states within energy bandgap in the proposed devices, the DOS was calculated based on the following equation [34]:

$$g(E_a) = -\frac{\varepsilon_i}{qd_i t \frac{dE_a}{dV_{GS}}} \quad (2)$$

where ε_i and d_i are, respectively, the permittivity and the thickness of the gate dielectric, q is the electron charge,

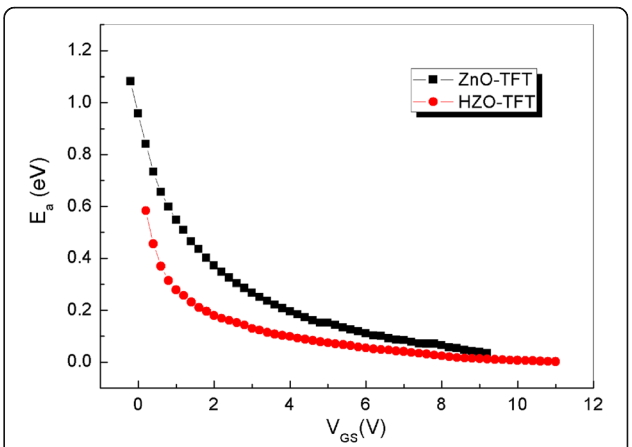

Fig. 6 Active energy (E_a) as a function of V_{GS}

and t is the thickness of the active layer. Figure 7 shows the DOS as a function of the energy (E_C–E) for ZnO-TFT and HZO-TFT, respectively. The total DOS for HZO-TFT is much smaller than that of ZnO-TFT, which matches with its falling rates. The total DOS value at a specific energy level is the summation of N_{it} and N_{SS} because both trap states hinder the moving up of the E_F level at the interface with increasing V_{GS} (>V_{FB}) [35]. Based on DOS results, we conclude that the ZnO-TFT has much more bulk traps and interface trap states than HZO-TFT. Therefore, the improved stability in HZO-TFT can be caused by the reduction in total traps causes. Using Hf doping is an effective way to suppress the generation of oxygen-vacancy-related defects and thus improve the stability of ZnO-based TFT.

Figure 8 displays the transfer curves of ZnO-TFT and HZO-TFT with gate bias of 10 V stress for an hour at room temperature. Threshold voltage shifts (ΔV_{th}) were 0.96 and 0.34 V for ZnO-TFT and HZO-TFT. HZO-TFT showed the smaller threshold voltage shift after 3600-s stress duration which indicates that it is more stable under bias stress than ZnO-TFT. Figure 9 shows the dependence of ΔV_{th} on the stress time. Lee reported [36] that the time dependence of ΔV_{th} is in agreement with a stretched-exponential equation, which can be expressed as:

$$\Delta V_{th}(t) = V_0\left\{1\text{-}\exp\left[-(t/\tau)^{\beta}\right]\right\} \quad (3)$$

where $V_0 = V_{GS}-V_{th,0}$, $V_{th,0}$ is the threshold voltage at the start of the stress measurement, β is the stretched exponential exponent, and τ reflects the characteristics of carrier trapping time. The obtained τ, β values are 1.58×10^6 s, 0.39 for ZnO-TFT, and 2.32×10^6 s, 0.56 for HZO-TFT, respectively. It demonstrates that the degradation of HZO-TFT is slower than that of ZnO-TFT under a long-time operation.

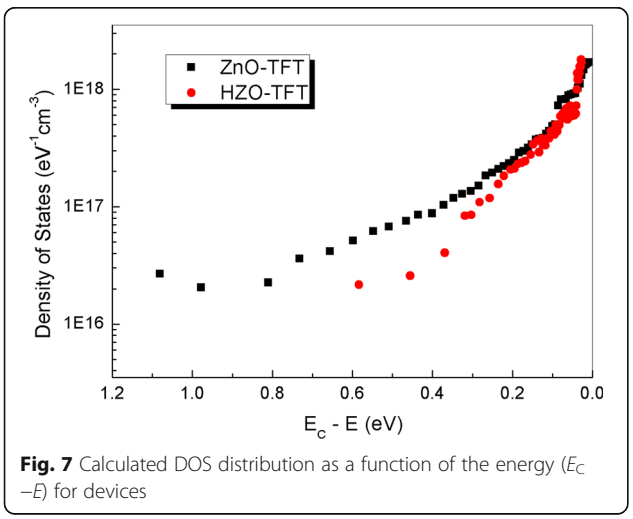

Fig. 7 Calculated DOS distribution as a function of the energy (E_C–E) for devices

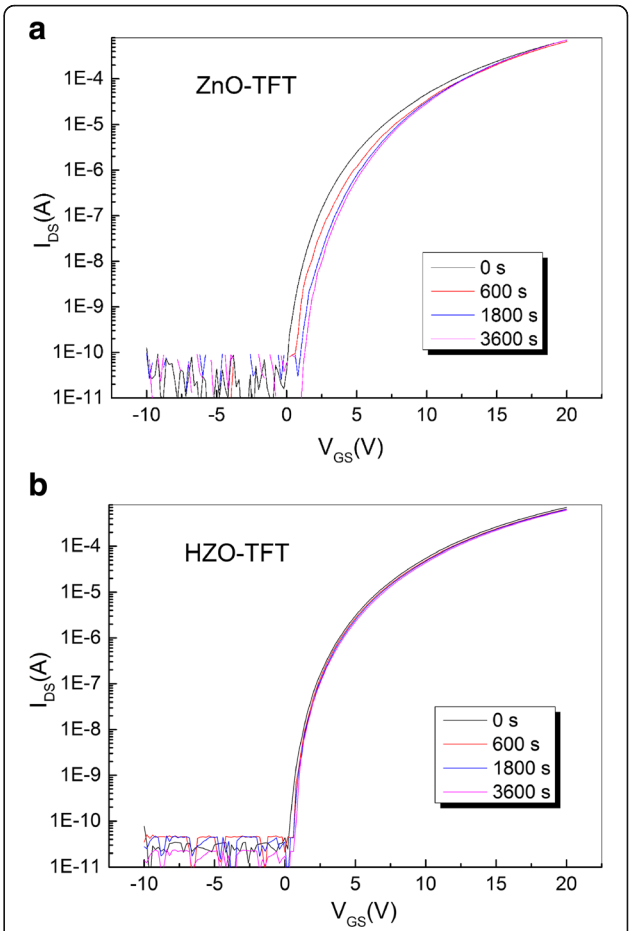

Fig. 8 The transfer curves of **a** ZnO-TFT and **b** HZO-TFT with gate bias of 10 V stress

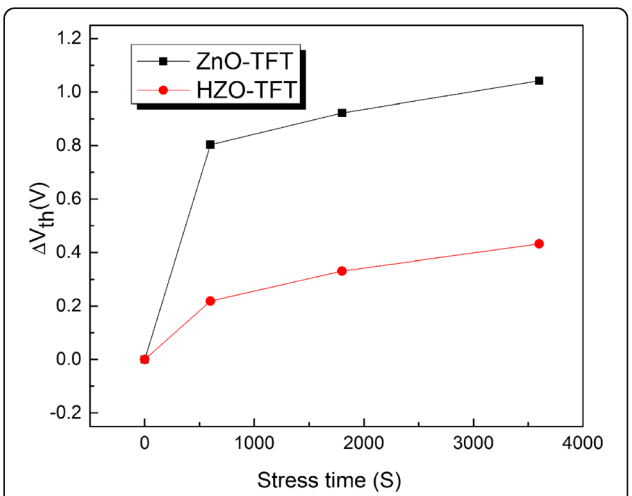

Fig. 9 The dependence of threshold voltage shift on stress time

Conclusions

In summary, we have successfully fabricated HZO-TFT via ALD, and the effect of Hf-doped ZnO on the stability of device was studied. Significantly improved on/off ratio and temperature stress stability were obtained in the HZO-TFT due to the reduced DOS, to be specific, a high field-effect mobility of 9.4 cm^2/Vs, a suitable turn-on voltage of 0.26 V, a high on/off ratio of over 10^7, a steep sub-threshold swing of 0.3 V/decade. The proposed HZO-TFT in this paper can act as driving devices in the next-generation flat panel displays.

Acknowledgements

This work is supported by the National Key Basic Research Program of China (2015CB655005), Science and Technology Commission of Shanghai Municipality Program (14DZ228090), Project of National Post-Doctor Fund (2015M580315) and National Natural Science Foundation of China (61077013, 61274082, 51072111, and 51302165).

Authors' Contributions

XD carried out the experiments and drafted the manuscript. XD and JZ participated in the design of the study and performed the analysis. CQ, JS participated in the measurements. XJ conceived the study and participated in its design. JZ and ZZ supervised the overall study and polished the manuscript. All authors read and approved the final manuscript

Competing Interests

The authors declare that they have no competing interests.

Author details

[1]Key Laboratory of Advanced Display and System Application, Ministry of Education, Shanghai University, 149 Yanchang Road, Jingan District, Shanghai 200070, People's Republic of China. [2]School of Mechatronics and Automation, Shanghai University, Shanghai 200072, China. [3]Department of Materials Science, Shanghai University, Shanghai 200072, China.

Received: 12 November 2016 Accepted: 17 January 2017
Published online: 23 January 2017

References

1. Nomura K, Ohta H, Takagi A, Kamiya T, Hosono H (2004) Room-temperature fabrication of transparent flexible thin-film transistors using amorphous oxide semiconductors. Nature (London) 432:488–492
2. Ji KH, Kim JI, Jung HY, Park SY, Mo YG, Jeong JH, Kwon JY, Ryu MK, Lee SY, Choi R, Jeong JK (2010) The effect of density-of-state on the temperature and gate bias-induced instability of InGaZnO thin film transistors. J Electrochem Soc 157:H983–H986
3. Namgung SD, Yang S, Park K, Cho A-J, Kim H, Kwon J-Y (2015) Influence of post-annealing on the off current of MoS_2 field-effect transistors. Nanoscale Res Lett 10:62
4. Wu J, Han DD, Cong YY, Zhao NN, Chen ZF, Dong JC, Zhao FL, Zhang SD, Liu LF, Zhang X, Wang Y (2015) Effects of channel thickness on characteristics of HZO-TFTs fabricated at low temperature. Electron Lett 51: 867–869
5. Nomura K, Ohta H, Ueda K, Kamiya T, Hirano M, Hosono H (2003) Thin-film transistor fabricated in single-crystalline transparent oxide semiconductor. Science 300:1269–1272
6. Ding X, Zhang H, Ding H, Zhang J, Huang C, Shi W, Li J, Jiang X, Zhang Z (2014) Growth of IZO/IGZO dual-active-layer for low-voltage-drive and high-mobility thin film transistors based on an ALD grown Al_2O_3 gate insulator. Superlattice Microst 76:156–162
7 Han CW, Kim KM, Bae SJ, Choi HS, Lee JM, Kim TS, Tak YH, Cha SY, Ahn BC (2012) 21.2: 55-inch FHD OLED TV employing New Tandem WOLEDs. SID Int Symp Dig Tech Pap 43:279–281
8 Rim YS, Kim SM, Kim KH (2008) Effects of substrate heating and film thickness on properties of silver-based ZnO multilayer thin films. Jpn J Appl Phys 47:5022–5027
9 Han DS, Park JH, Kang YJ, Park JW (2013) Improvement in the bias stability of zinc-tin oxide thin-film transistors by hafnium doping. J Electron Mater 42:2470–2477
10 Kim C-J, Kim S, Lee J-H, Park J-S, Kim S, Park J, Lee E, Lee J, Park Y, Kim JH, Shin ST, Chung U-I (2009) Amorphous hafnium-indium-zinc oxide semiconductor thin film transistors. Appl Phys Lett 95:252103
11 Chong E, Jo KC, Lee SY (2010) High stability of amorphous hafnium-indium-zinc-oxide thin film transistor. Appl Phys Lett 96:152102
12 Ahn CH, Yun MG, Lee SY, Cho HK (2014) Enhancement of electrical stability in oxide thin-film transistors using multilayer channels grown by atomic layer deposition. IEEE T Electron Dev 61:73–78
13 Hosono H (2006) Ionic amorphous oxide semiconductors: Material design, carrier transport, and device application. J Non-Cryst Solids 352:851–858
14 Ahn CH, Kong BH, Kim H, Cho HK (2011) Improved electrical stability in the Al doped ZnO thin-film-transistors grown by atomic layer deposition. J Electrochem Soc 158:H170–H173
15 Shih H-Y, Chu F-C, Das A, Lee C-Y, Chen M-J, Lin R-M (2016) Atomic layer deposition of gallium oxide films as gate dielectrics in AlGaN/GaN metal-oxide-semiconductor high-electron-mobility transistors. Nanoscale Res Lett 11:1–9
16 Zheng L-L, Ma Q, Wang Y-H, Liu W-J, Ding S-J, Zhang DW (2016) High-Performance unannealed a-InGaZnO TFT with an Atomic-Layer-Deposited SiO_2 insulator. IEEE Electr Device L 37:743–746
17 Puurunen RL (2005) Surface chemistry of atomic layer deposition: a case study for the trimethylaluminum/water process. J Appl Phys 97:121301
18 Park J-S, Kim H, Kim I-D (2014) Overview of electroceramic materials for oxide semiconductor thin film transistors. J Electroceram 32:117–140
19 Park JS, Maeng W-J, Kim H-S, Park J-S (2012) Review of recent developments in amorphous oxide semiconductor thin-film transistor devices. Thin Solid Films 520:1679–1693
20 Kim C-J, Kim S, Lee J-H, Park J-S, Kim S, Park J, Lee E, Lee J, Park Y, Kim JH, Shin ST, Chung U-I (2009) Amorphous hafnium-indium-zinc oxide semiconductor thin film transistors. Appl Phys Lett 95:252103
21 Kim W-S, Moon Y-K, Kim K-T, Shin S-Y, Ahn BD, Lee J-H, Park J-W (2011) The influence of hafnium doping on bias stability in zinc oxide thin film transistors. Thin Solid Films 519:5161–5164
22 Li C-H, Chen J-Z, Cheng I-C (2013) Transitions of bandgap and built-in stress for sputtered HfZnO thin films after thermal treatments. J Appl Phys 114: 084503
23 Li C-H, Chen J-Z (2014) Electrical, optical, and microstructural properties of sol–gel derived HfZnO thin films. J Alloy Compd 601:223–230
24 Kim W-S, Moon Y-K, Kim K-T, Shin S-Y, Ahn BD, Lee J-H, Park J-W (2011) Improvement in the negative bias temperature stability of ZnO based thin film transistors by Hf and Sn doping. Thin Solid Films 519:6849–6852
25 Kim W-S, Moon Y-K, Kim K-T, Shin S-Y, Ahn BD, Lee J-H, Park J-W (2010) The influence of the hafnium doping on negative bias stability in zinc oxide thin film transistor. Electrochem Solid-State Lett 13:H295–H297
26 Kim Y-S, Park CH (2009) Rich variety of defects in ZnO via an attractive interaction between O vacancies and Zn interstitials: origin of n-type doping. Phys Rev Lett 102:086403
27 Kofstad P (1962) Studies of electrical conductivity of Nb2O5 as a function of oxygen pressure at 600–1200°C. J Phys Chem Solids 23:1571–1578
28 Gavryushin V, Ra˘ciukaitis G, Juodžbalis D, Kazlauskas A, Kubertavi˘cius V (1994) Characterization of intrinsic and impurity deep levels in ZnSe and ZnO crystals by nonlinear spectroscopy. J Cryst Growth 138:924–933
29 Takechi K, Nakata M, Eguchi T, Yamaguchi H, Kaneko S (2009) Comparison of ultraviolet photo-field effects between hydrogenated amorphous silicon and amorphous InGaZnO4 thin-film transistors. J Appl Phys 48:011301
30 Gavryushin V, Raciukaitis G, Juodzbalis D, Kazlauskas A, Kubertavicius V (1994) Characterization of intrinsic and impurity deep levels in ZnSe and ZnO crystals by nonlinear spectroscopy. J Cryst Growth 138:924–933
31 Indluru A, Alford TL (2010) High-temperature stability and enhanced performance of a-Si: H TFT on flexible substrate due to improved interface quality. IEEE T Electron Dev 57:3006–3011
32 Pichon L, Mercha A, Carin R, Bonnaud O, Mohammed-Brahim T, Helen Y, Rogel R (2000) Analysis of the activation energy of the subthreshold current in laser-and solid-phase-crystallized polycrystalline silicon thin-film transistors. Appl Phys Lett 77:576
33 Tai YH, Chiu HL, Chou LS (2012) The deterioration of a-IGZO TFTs owing to the copper diffusion after the process of the source/drain metal formation. J Electrochem Soc 159:J200–J203

34 Jeong JK, Yang S, Cho D-H, Park S-HK, Hwang C-S, Cho KI (2009) Impact of device configuration on the temperature instability of Al–Zn–Sn–O thin film transistors. Appl Phys Lett 95:123505
35 Chang G-W, Chang T-C, Jhu J-C, Tsai T-M, Syu Y-E, Chang K-C, Jian F-Y, Hung Y-C, Tai Y-H (2013) N_2O plasma treatment suppressed temperature-dependent sub-threshold leakage current of amorphous indium–gallium–zinc-oxide thin film transistors. Surf Coat Tech 231:281–284
36 Lee JM, Cho IT, Lee JH, Kwon HI (2008) Bias-stress-induced stretched-exponential time dependence of threshold voltage shift in InGaZnO thin film transistors. Appl Phys Lett 93:093504